DEPARTMENT OF STATISTICS
University of Wisconsin
1210 West Dayton St.
Madison, WI 53706

TECHNICAL REPORT NO. 1049

January 1, 2002

Tensor-Based Surface Morphometry

Moo K. Chung [1]
Department of Statistics, University of Wisconsin, Madison, WI

Keith J. Worsley
Department of Mathematics and Statistics, McGill University, Canada

Tomas Paus, Steve Robbins, Alan C. Evans
Montreal Neurological Institute, McGill University, Canada

Jonathan Taylor
Department of Statistics, Stanford University, Stanford, CA

Jay N. Giedd, Judith L. Rapoport
Child Psychiatry Branch, National Institute of Mental Health, Bethesda, MD

[1]email://mchung@stat.wisc.edu, http://www.stat.wisc.edu/~mchung

Abstract

We present a unified statistical approach to deformation-based morphometry applied to the cortical surface. The cerebral cortex has the topology of a 2D highly convoluted sheet. As the brain develops over time, the cortical surface area, thickness, curvature and total gray matter volume change. It is highly likely that such age-related surface deformations are not uniform. By measuring how such surface metrics change over time, the regions of the most rapid structural changes can be localized. By formulating the surface deformation in tensor geometry, surface flattening, which distorts the inherent geometry of the cortex, can be avoided. To increase the signal to noise ratio, diffusion smoothing, which generalizes Gaussian kernel smoothing to an arbitrary curved cortical surface, has been developed and applied to surface data. Afterwards, statistical inference on the cortical surface will be performed via random fields theory. As an illustration, we demonstrate how this new surface-based morphometry can be applied in localizing the cortical regions of the gray matter tissue growth and loss in the brain images longitudinally collected in the group of children and adolescents.

Keywords: Cerebral Cortex, Cortical Surface, Brain Development, Cortical Thickness, Brain Growth, Brain Atrophy

1 Introduction

The cerebral cortex has the topology of a 2-dimensional convoluted sheet. Most of the features that distinguish these cortical regions can only be measured relative to that local orientation of the cortical surface (Dale and Fischl, 1999). As brain develops over time, cortical surface area as well as cortical thickness and the curvature of the cortical surface change. As shown in the previous normal brain development studies, the growth pattern in developing normal children is nonuniform over whole brain volume (Chung *et al.*, 2001; Giedd *et al.*, 1999; Paus *et al.*, 1999, Thompson *et al.*, 2000). Between ages 12 and 16, the corpus callosum and the temporal and parietal lobes shows the most rapid brain tissue growth and some tissue degeneration in the subcortical regions of the left hemisphere (Chung *et al.* 20001, Thompson *et al.*, 2001). It is equally likely that such age-related changes with respect to the cortical surface are not uniform as well. By measuring how geometric metrics such as the cortical thickness, curvature and local surface area change over time, any statistically significant brain tissue growth or loss in the cortex can be detected.

The first obstacle in developing surfaced-based morphometry is the automatic segmentation or extraction of the cortical surfaces from MRI. It requires first the tissue classification into three types: gray matter, white matter and cerebrospinal fluid (CSF). An artificial neural network classifier (Ozkan *et al.*, 1993) or a mixture model cluster analysis (Good *et al.*, 2001) can be used to segment the tissue types automatically. After the tissue classification, the cortical surface is usually generated as a continuous triangular mesh topologically equivalent to a sphere. The most widely used method for triangulating the surface is the marching cubes algorithm (Lorensen and Cline, 1987). Level set method (Sethian, 1996) or deformable surfaces method (Davatzikos, 1995) are also available. In our study, we have used the anatomic segmentation using proximities (ASP) method (MacDonald *et al.*, 2000), which is a variant of the deformable surfaces method, to generate cortical triangular meshes consisting of 81,920 triangles each. Once we have a triangular mesh as the realization of the cortical surface, we can mathematically model how the cortical surface deforms over time.

In modeling the surface deformation, a proper mathematical framework can be found in both differential geometry and fluid dynamics. The concept of the *evolution of phase-*

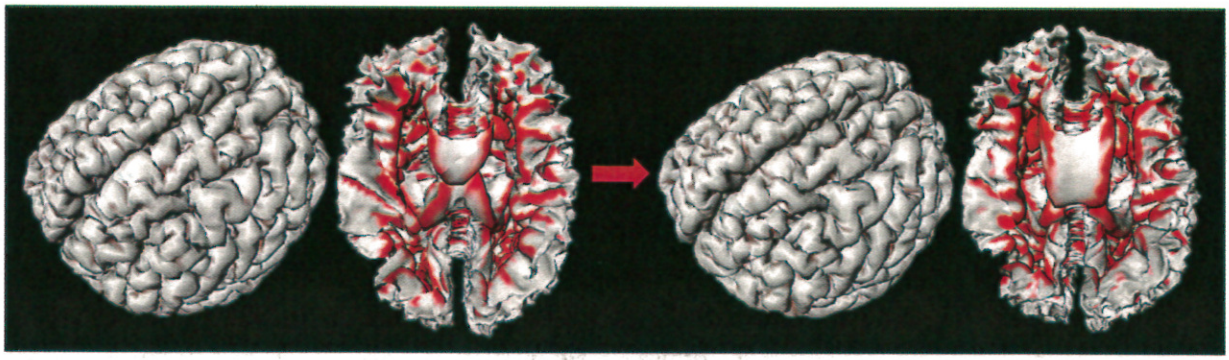

Figure 1: The outer and inner cortical surfaces of a single subject at age 14 (left) and at age 19 (right) showing globally similar cortical patterns. The top of the inner cortical surface has been removed to show predominant ventricle enlargement. The red color is the region where the mean curvature is greater than 0.01.

boundary in fluid dynamics (Drew, 1991; Gurtin and McFadden, 1991), which describes the geometric properties of the evolution of boundary layer between two different materials due to internal growth or external force, can be used to derive the mathematical formula for surface deformation. It is natural to assume the cortical surfaces to be a smooth 2-dimensional *Riemannian manifold* parameterized by u^1 and u^2:

$$X(u^1, u^2) = \{x_1(u^1, u^2), x_2(u^1, u^2), x_3(u^1, u^2) : (u^1, u^2) \in D \subset \mathbb{R}^2\}.$$

A more precise definition of a Riemannian manifold and a *parameterized surface* can be found in Boothby (1986), Carmo (1992) and Kreyszig (1959). If D is a unit square in $\mathbb{R}^2$ and a surface is topologically equivalent to a sphere then at least two different global parameterizations are required. Surface parameterization of the cortical surface bas been done previously by Thompson and Toga (1996) and Joshi *et al.* (1995). From the surface parameterization, Gaussian and mean curvatures of the brain surface can be computed and used to characterize its shape (Dale and Fischl, 1999; Griffin, 1994; Joshi *et al.*, 1995). In particular, S.C. Joshi *et al.* (1995) used the quadratic surface in estimating the Gaussian and mean curvature of the cortical surfaces.

By combining the mathematical framework of the evolution of phase-boundary with the statistical framework developed for 3D whole brain volume deformation (Chung *et al.*, 2001), anatomical variations associated with the deformation of the cortical surface can be statistically quantified. Using the same stochastic assumption on the deformation field used

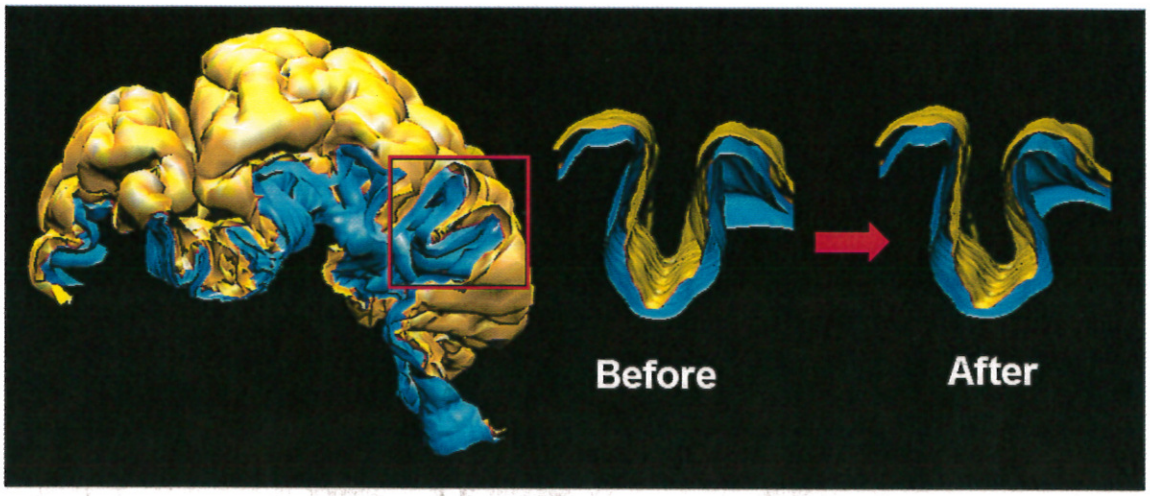

Figure 2: Yellow: outer cortical surface, blue: inner cortical surface. Gray matter deformation causes the geometry of the both outer and inner cortical surface to change. The deformation of the surfaces can be written as $\mathbf{x} \rightarrow \mathbf{x} + \mathbf{U}(\mathbf{x}, t)$, where $\mathbf{U}$ is the surface displacement vector field.

in Chung *et al.* (2001), we derive the statistical distributions of morphological metrics such as area dilatation rate, cortical thickness and curvature changes. These statistics will be used in statistical inferences on the cortical surface.

As an illustration of our unified approach to surface-based morphometry, we will demonstrate how the surface-based statistical analysis can be applied in localizing the cortical regions of tissue growth and loss in brain images longitudinally collected in a group of children and adolescents.

2 Modeling Surface Deformation

Let $\mathbf{U}(\mathbf{x}, t) = (U_1, U_2, U_3)^t$ be the 3D displacement vector required to deform the structure at $\mathbf{x} = (x_1, x_2, x_3)$ in gray matter Ω_0 to the homologous structure after time t. Whole gray matter volume Ω_0 will deform continuously and smoothly to Ω_t via the deformation $\mathbf{x} \rightarrow \mathbf{x} + \mathbf{U}$ while the cortical boundary $\partial\Omega_0$ will deform to $\partial\Omega_t$. The cortical surface $\partial\Omega_t$ may be considered as consisting of two parts: the outer cortical surface $\partial\Omega_t^{out}$ between the gray matter and CSF and the inner cortical surface $\partial\Omega_t^{in}$ between the gray and white matter (Figure 2), i.e.

$$\partial\Omega_t = \partial\Omega_t^{out} \cup \partial\Omega_t^{in}.$$

Although we will exclusively deal with the deformation of the cortical surfaces, our tensor-based surface morphometry can be equally applicable to the boundary of any brain substructure. We propose the following stochastic model on the displacement velocity $\mathbf{V} = \partial \mathbf{U}/\partial t$, which has been used in the analysis of whole brain volume deformation (Chung *et al.*, 2001):

$$\mathbf{V}(\mathbf{x}) = \mu(\mathbf{x}) + \Sigma^{1/2}(\mathbf{x})\epsilon(\mathbf{x}), \mathbf{x} \in \Omega_0, \tag{1}$$

where μ is the mean displacement velocity and $\Sigma^{1/2}$ is the 3×3 symmetric positive definite covariance matrix, which allows for correlations between components of the displacement fields. The components of the error vector ϵ are are assumed to be independent and identically distributed as smooth stationary Gaussian random fields with zero mean and unit variance. It can be shown that the normal component of the displacement velocity $\mathbf{V} = \partial \mathbf{U}/\partial t$ restricted on the boundary $\partial\Omega_0$ uniquely determine the evolution of the cortical surface. Assuming the surface $\partial\Omega_t$ to be smooth enough, it can be *locally* expressed in an implicit form

$$F(\mathbf{x}, t) = 0, \mathbf{x} \in \partial\Omega_t \tag{2}$$

By taking the time derivative in (2), the *kinematic equation* for the surface deformation is given by

$$\frac{\partial F}{\partial t} + \langle \mathbf{V}, \nabla F \rangle = 0, \tag{3}$$

where $\nabla F = \left(\frac{\partial F}{\partial x_1}, \frac{\partial F}{\partial x_2}, \frac{\partial F}{\partial x_3}\right)^t$ is the gradient vector and $\langle , \rangle$ is the inner product (Drew, 1991). The unit normal vector to the surface is given by

$$\mathbf{n} = \frac{\nabla F}{\|\nabla F\|}. \tag{4}$$

From (3) and (4), the kinematic equation becomes

$$\frac{\partial F}{\partial t} = -\|\nabla F\| \mathbf{V_n}, \tag{5}$$

where $\mathbf{V_n} = \langle \mathbf{V}, \mathbf{n} \rangle$ is the normal component of the surface displacement velocity. If we let $\mathbf{V_t}$ denote the tangential component of $\mathbf{V}$, then $\mathbf{V} = \mathbf{V_n} + \mathbf{V_t}$. There are infinitely many surface displacement velocities that gives the same normal component $\mathbf{V_n}$ and in turn, the same kinematic equation (5), which describes the evolution of the cortical surface over time.

Hence, the translation of the surface in the tangential direction does not change the geometry of the surface and only the normal component $\mathbf{V_n}$ uniquely determines the evolution of the cortical surface at a given point for small time interval. This concept will play an important role in modeling surface curvature change later.

3 Surface Parameterization

In our analysis, we have used the anatomic segmentation using proximities (ASP) method (MacDonald *et al.*, 2000), which is a variant of the deformable surfaces method, to extract the cortical surfaces from T_1-weighted MRIs. The ASP method generates 81,920 triangles evenly distributed in size. In order to perform a statistical analysis on the cortical surface, *surface parameterization* is an essential part. We model the cortical surface as a smooth 2D Riemannian manifold parameterized by two parameters u^1 and u^2 such that any point $\mathbf{x} \in \partial\Omega_0$ can be uniquely represented as

$$\mathbf{x} = X(u^1, u^2)$$

for some parameter space $\mathbf{u} = (u^1, u^2) \in D \subset \mathbb{R}^2$. We will try to avoid global parameterization such as tensor B-splines, which are computationally expensive compared to a local surface parameterization. Instead, a quadratic polynomial

$$z(u^1, u^2) = \beta_1 u^1 + \beta_2 u^2 + \beta_3 (u^1)^2 + \beta_4 u^1 u^2 + \beta_5 (u^2)^2$$

will be used as a local parameterization fitted via least-squares estimation. Using the least-squares method, these coefficients β_i can be estimated. The numerical implementation can be found in Chung (2001). Slightly different quadratic surface parameterizations are also used in estimating curvatures of a macaque monkey brain surface (Joshi *et al.*, 1995; Khaneja *et al.*, 1998). Once β_i are estimated, $X(u^1, u^2) = \left(u^1, u^2, z(u^1, u^2)\right)^t$ is a local surface parameterization we will use.

4 Surface-Based Morphological Measures

4.1 Metric Tensor Change

As in the case of local volume change in the whole brain volume (Chung *et al.*, 2001), the rate of cortical surface area expansion or reduction may not be uniform across the cortical surface. Extending the idea of volume dilatation, we introduce a new concept of surface area, curvature, cortical thickness dilatation and its rate of change over time via tensor geometry.

Suppose that the cortical surface $\partial\Omega_t$ at time t can be parameterized by the parameters $\mathbf{u} = (u^1, u^2)$ such that any point $\mathbf{x} \in \partial\Omega_t$ can be written as $\mathbf{x} = X(\mathbf{u}, t)$. Let $X_i = \partial X/\partial u^i$ be a partial derivative vector. The *Riemannian metric tensor* g_{ij} is given by the inner product between two vectors X_i and X_j, i.e. $g_{ij}(t) = \langle X_i, X_j \rangle$. The Riemannian metric tensor g_{ij} measures the amount of the deviation of the cortical surface from a flat Euclidean plane. Note that g_{ij} is a function of both space and time, i.e. $g_{ij} = g(\mathbf{x}, t)$ but as it is standard in tensorial computation, the spatial coordinates $\mathbf{x}$ will be omitted if there is no ambiguity. The Riemannian metric tensor enables us to measure lengths, angles and areas in the cortical surface. Let $g = (g_{ij})$ be a 2×2 matrix of metric tensors. From Appendix A, the rate of metric tensor change is approximately

$$\frac{\partial g}{\partial t} \approx 2(\nabla X)^t (\nabla \mathbf{V}) \nabla X, \tag{6}$$

where $\mathbf{V} = \partial \mathbf{U}/\partial t$ and $\nabla X = (X_1, X_2)|_{t=0}$ is a 3×2 gradient matrix evaluated at $t = 0$. We are not directly interested in the metric tensor change itself but rather functions of g or $\partial g/\partial t$, which will be used to measure surface area and curvature change.

4.2 Local Surface Area Change

The *infinitesimal surface area element* (Kreyszig, 1959) [28, pp. 114] is defined as

$$\sqrt{\det g} = (g_{11}g_{22} - g_{12}^2)^{1/2}. \tag{7}$$

It measures the transformed area of the unit square in the parameter space D via the transformation $X(\cdot, t) : D \to \partial\Omega_t$ and it is a generalization of Jacobian, which has been used

in measuring local volume in whole brain volume (Chung *et al.*, 2001). The *local surface area dilatation rate* Λ_{area} or the rate of local surface area change per unit surface area is then

$$\Lambda_{area} = \frac{\partial}{\partial t} \ln \sqrt{\det g} = \frac{1}{2 \det g} \frac{\partial (\det g)}{\partial t}.$$

If the whole gray matter Ω_t is parameterized by 3D curvilinear coordinates $\mathbf{u} = (u^1, u^2, u^3)$, then the dilatation rate $\partial(\ln \sqrt{\det g})/\partial t$ becomes the local volume dilatation rate Λ_{volume} first introduced in *deformation-based morphometry* (Chung *et al.*, 2001). Therefore, the concepts of local area dilatation and volume dilatation rates are equivalent in tensor geometry. A simple matrix manipulation in Harville (1999, pp. 304-308) shows that

$$\Lambda_{area} = \frac{1}{2} \mathrm{tr}\Big(g^{-1} \frac{\partial g}{\partial t} \Big). \tag{8}$$

From (6) and (8), the rate of local surface area change becomes

$$\Lambda_{area} \approx \mathrm{tr}[g^{-1} (\nabla X)^t (\frac{\partial}{\partial t} \nabla \mathbf{U}) \nabla X].$$

Since the partial derivatives of Gaussian random fields are again Gaussian (Adler, 1981, pp. 33), under the assumption of stochastic model (1), the area dilatation rate is then distributed as Gaussian:

$$\Lambda_{area}(\mathbf{x}) = \lambda_{area}(\mathbf{x}) + \epsilon_{area}(\mathbf{x}), \tag{9}$$

where $\lambda_{area} = tr[g^{-1} (\nabla X)^t (\nabla \mu) \nabla X]$ is the mean area dilatation rate and ϵ_{area} is a mean zero Gaussian random field defined on the cortical surface. The area dilatation rate is invariant under parameterization, i.e. the area dilatation rate will always be the same no matter which parametrization is chosen. Afterwards, statistical inference on local surface area expansion or reduction can be performed via the T random field defined on the cortical surface (Worsley *et al.*, 1996a; Worsley *et al.*, 1999). In order to apply the random field theory developed in Worsley *et al.* (1996a) and Worsley *et al.* (1999), it is assumed that $\mathbf{Var}(\epsilon_{area})$ is independent of t. So far our statistical modeling is concentrated on localizing regions of rapid morphological changes on the cortical surface but both local and global morphological measures are important in the characterization of brain deformation. Global morphometry is relatively easy compared to local morphometry with respect to modeling

and computation. The total surface area of the cortex $\partial\Omega_t$ is given by

$$\|\partial\Omega_t\| = \int_D \sqrt{\det(g)}\, d\mathbf{u},$$

where $D = X^{-1}(\partial\Omega_t)$ and g is the metric matrix corresponding to the global parameterization $X(\mathbf{u})$. $\|\partial\Omega_t\|$ can be estimated by the sum of the areas of 81,920 triangles generated by the ASP algorithm. Then we define the total surface area dilatation rate as

$$\Lambda_{total\ area} = \frac{\partial}{\partial t} \ln \|\partial\Omega_t\| \Big|_{t=0}.$$

It can be shown that, under assumption (1), the total surface area dilatation rate $\Lambda_{total\ area}$ is distributed as a Gaussian random variable and hence a statistical inference on total surface area change will be based on a simple t test. This measure will be used in determining the rate of the total surface area decreases in both outer and inner cortical surfaces between ages 12 and 16.

4.3 Cortical Thickness Change

The average cortical thickness for each individual is about 3mm (Henery and Mayhew, 1989). Cortical thickness usually varies from 1mm to 4mm depending on the location of the cortex. In normal brain development, it is highly likely that the change of cortical thickness may not be uniform across the cortex. We will show how to localize the cortical regions of statistically significant thickness change in brain development. Our approach introduced here can also be applied to measuring the rate of cortical thinning, possibly associated with Alzheimer's disease. As in the case of the surface area dilatation, we introduce the concept of the cortical thickness dilatation, which measures cortical thickness change per unit thickness and unit time. There are many different computational approaches to measuring cortical thickness but we will use the Euclidean distance $d(\mathbf{x})$ from a point $\mathbf{x}$ on the outer surface $\partial\Omega_t^{out}$ to the corresponding point $\mathbf{y}$ on the inner surface $\partial\Omega_t^{in}$, as defined by the automatic linkages used in the ASP algorithm (MacDonald *et al.* , 2000). A validation study for the assessment of the accuracy of the cortical thickness measure based on the ASP algorithm has been performed and found to be valid for the most of the cortex (Kanani *et al.*, 2000). There is

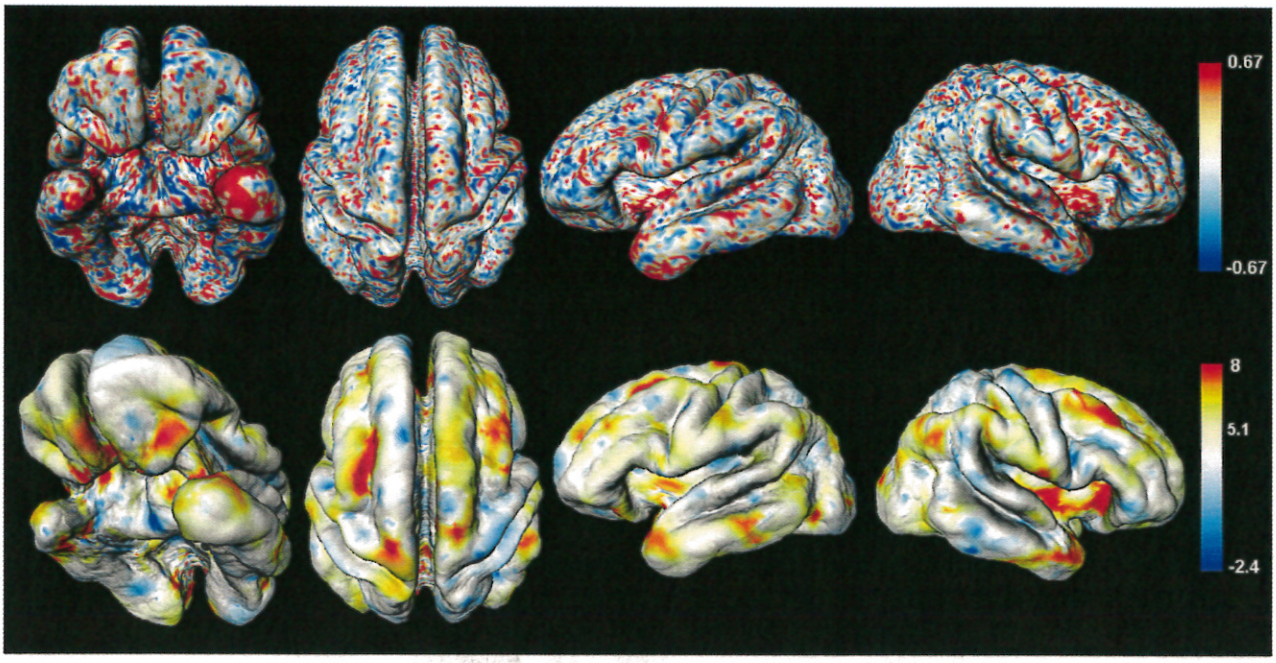

Figure 3: Top: Cortical thickness dilatation rate for a single subject mapped onto an atlas. The red (blue) regions show more than 67% thickness increase (decrease). Note the large variations across the cortex. Due to such large variations, surface-based smoothing is required to increase the signal-to-noise ratio. Bottom: t statistical map thresholded at the corrected P value of 0.05 (t value of 5.1). Both yellow and red regions are statistically significant regions of thickness increase. There is no region of statistically significant cortical thinning detected. The blue region shows very small t value of -2.4, which is not statistically significant.

also an alternate method for automatically measuring cortical thickness based on the Laplace equation (Jones *et al.*, 2000).

Let $d(\mathbf{x}) = \|\mathbf{x} - \mathbf{y}\|$ be the cortical thickness computed as usual Euclidean distance between $\mathbf{x} \in \partial\Omega^{out}$ and $\mathbf{y} \in \partial\Omega^{in}$. We define the *cortical thickness dilatation rate* as the rate of the change of the thickness per unit thickness and unit time, i.e.

$$\Lambda_{thickness} = \frac{\partial}{\partial t} \ln d(\mathbf{X}).$$

Under the assumption of stochastic model (1) and Appendix B, we have a linear model on the thickness dilatation rate given by

$$\Lambda_{thickness}(\mathbf{x}) = \lambda_{thickness}(\mathbf{x}) + \epsilon_{thickness}(\mathbf{x}),$$

where $\lambda_{thickness}$ is the mean cortical thickness dilatation rate and $\epsilon_{thickness}$ is a mean zero Gaussian random field. Therefore, the statistical inference on the cortical thickness change can be again based on the T random field.

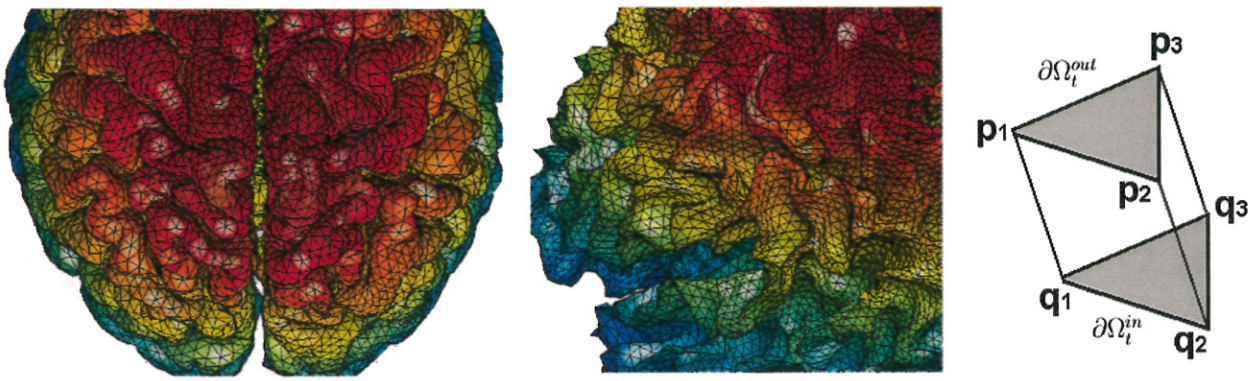

Figure 4: Outer (left) and inner (middle) triangular meshes. Triangle $(\mathbf{p}_1, \mathbf{p}_2, \mathbf{p}_3) \in \partial\Omega_t^{out}$ on the outer surface will have corresponding triangle $(\mathbf{q}_1, \mathbf{q}_2, \mathbf{q}_3) \in \partial\Omega_t^{in}$ on the inner surface. A convex-hull from 6 points $\{\mathbf{p}_1, \mathbf{p}_2, \mathbf{p}_3, \mathbf{q}_1, \mathbf{q}_2, \mathbf{q}_3\}$ will then form a triangular prism and a collection of 81,920 triangular prisms become the whole gray matter.

4.4 Local Gray Matter Volume Change

Local volume dilatation rate Λ_{volume} for whole brain volume is defined in Chung *et al.* (2001) using Jacobian of deformation $\mathbf{x} \rightarrow \mathbf{x} + \mathbf{U}(\mathbf{x})$. Compared to the local surface area change measurement, the local volume change measurement is more sensitive to small deformation. If a unit cube increases its sides by one, the surface area will increase by $2^2 - 1 = 3$ while the volume will increase by $2^3 - 1 = 7$. Therefore, the statistical analysis based on the local volume change will be at least twice more sensitive compared to that of the local surface area change. So the local volume change should be able to pick out gray matter tissue growth pattern even when the local surface area change may not. In Result section, the highly sensitive aspect of local volume change in relation to local surface area change will be demonstrated.

Similar to the total surface area dilatation rate, we define the total gray matter volume dilatation rate. The gray matter Ω_t can be considered as a thin shell bounded by two surfaces $\partial\Omega_t^{out}$ and $\partial\Omega_t^{in}$ with varying cortical thickness $d(\mathbf{x})$. Then the total gray matter volume is approximately

$$\|\Omega_t\| \approx \int_{\partial\Omega_t^{out}} d(\mathbf{x})\, d\mathbf{x}. \tag{10}$$

with respect to the outer cortical surface. Let us define the total gray matter volume dilata-

tion rate as

$$\Lambda_{total\ volume} = \frac{\partial}{\partial t} \ln \|\Omega_t\| \Big|_{t=0}.$$

It can be shown that

$$\Lambda_{total\ volume} \approx \frac{1}{\|\Omega_0\|} \int_{\Omega_0} \Lambda_{volume}\, d\mathbf{x},$$

where $\Lambda_{volume} = \mathrm{tr}(\nabla \mathbf{V})$ is the local volume dilatation rate distributed as a mean zero Gaussian random field (Chung *et al.*, 2001). Therefore, under the assumption of (1), the total volume dilatation rate of the gray matter is distributed as a Gaussian random variable.

In triangular meshes generated by ASP algorithm, each of 81,920 triangles on the outer surface has a corresponding triangle on the inner surface (Figure 4). Let $\mathbf{p}_1, \mathbf{p}_2, \mathbf{p}_3$ be the three vertices of a triangle on the outer surface and $\mathbf{q}_1, \mathbf{q}_2, \mathbf{q}_3$ be the corresponding three vertices on the inner surface such that $\mathbf{p}_i$ is linked to $\mathbf{q}_i$ by ASP algorithm. The triangular prism consists of three tetrahedra with the vertices $\{\mathbf{p}_1, \mathbf{p}_2, \mathbf{p}_3, \mathbf{q}_1\}$, $\{\mathbf{p}_2, \mathbf{p}_3, \mathbf{q}_1, \mathbf{q}_2\}$ and $\{\mathbf{p}_3, \mathbf{q}_1, \mathbf{q}_2, \mathbf{q}_3\}$. Then the volume of the triangular prism is given by the sum of the determinants

$$D(\mathbf{p}_1, \mathbf{p}_2, \mathbf{p}_3, \mathbf{q}_1) + D(\mathbf{p}_2, \mathbf{p}_3, \mathbf{q}_1, \mathbf{q}_2) + D(\mathbf{p}_3, \mathbf{q}_1, \mathbf{q}_2, \mathbf{q}_3),$$

where $D(\mathbf{a}, \mathbf{b}, \mathbf{c}, \mathbf{d}) = |\det(\mathbf{a} - \mathbf{d}, \mathbf{b} - \mathbf{d}, \mathbf{c} - \mathbf{d})|/6$ is the volume of a tetrahedron whose vertices are $\{\mathbf{a}, \mathbf{b}, \mathbf{c}, \mathbf{d}\}$. Afterwards, the total volume $\|\Omega_t\|$ can be estimated by summing the volumes of all 81,920 triangular prisms.

4.5 Curvature Change

When the surface $\partial\Omega_0$ deforms to $\partial\Omega_t$, curvatures of the surface change as well. The *principal curvatures* can characterize the shape and location of the sulci and gyri, which are the valleys and crests of the cortical surfaces (Bartesaghi *et al.*, 2001; Joshi *et al.*, 1995; Khaneja *et al.*, 1998; Subsol, 1999). By measuring the curvature changes, rapidly folding and unfolding cortical regions can be localized. Let κ_1 and κ_2 be the two principal curvatures as defined in Boothby (1986) and Kreyszig (1959). From Shi (2000), the local bending energy of an ideal thin plate is defined as

$$K = \frac{\kappa_1^2 + \kappa_2^2}{2}.$$

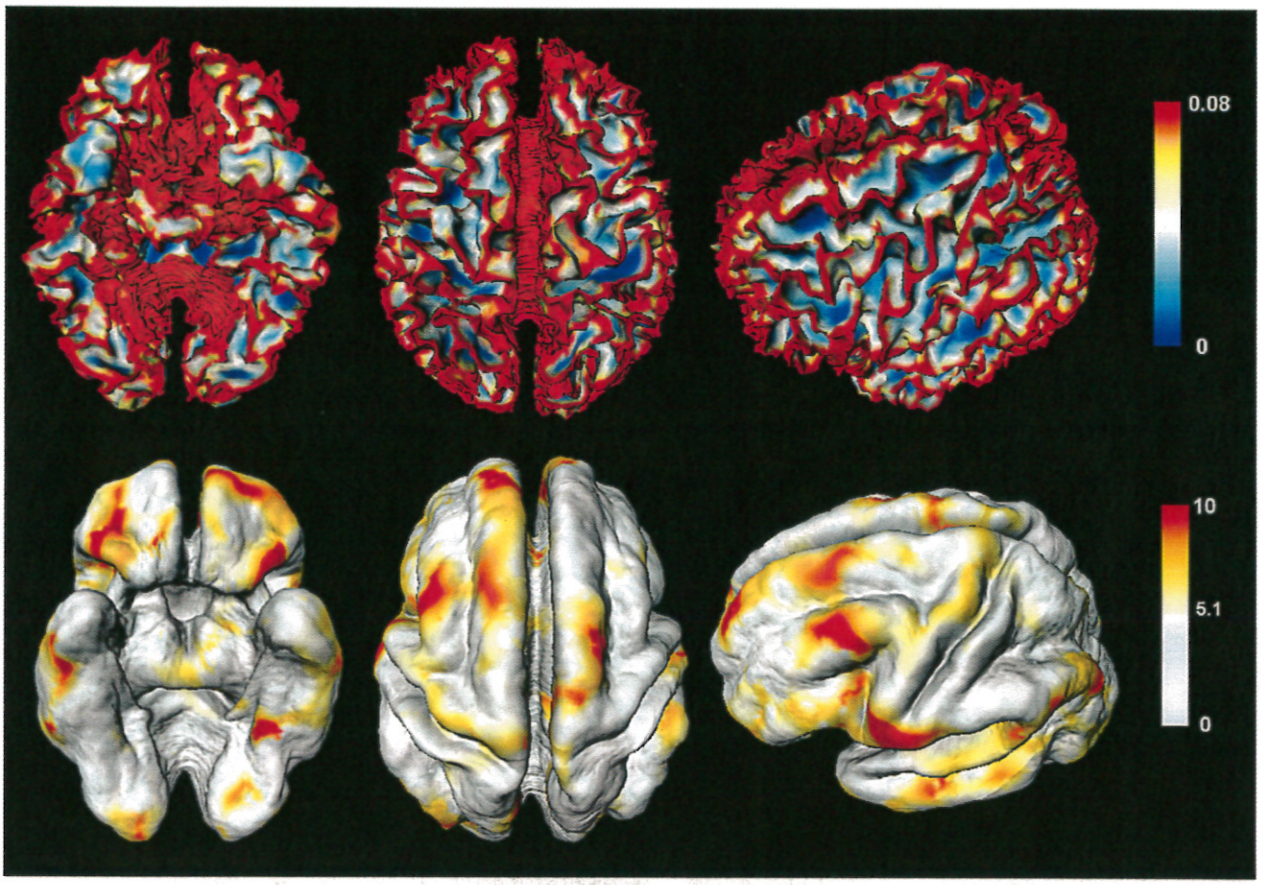

Figure 5: Top: Bending energy computed on the inner cortical surface of a 14 year old subject. It measures the amount of folding or curvature of the cortical surface. This metric can be also used to extract sulci and gyri in the problem of sulcal segmentation. Bottom: Corrected t map thresholded at 5.1 showing statistically significant region of curvature increase. Most of curvature increase occurs on gyri while there is no significant change of curvature on most of sulci. Also there is *no* statistically significant curvature decrease detected indicating that the complexity of the surface convolution may actually increase between ages 12 and 16.

K could be any number between 0 and infinity and it measures the amount of curvature at a given point. If the cortical surface is flat, the bending energy K vanishes. The larger the bending energy, the more surface will be crested (Figure 5). We define the *local curvature dilatation rate* as

$$\Lambda_{curvature} = \frac{\partial}{\partial t} \ln K. \tag{11}$$

Under the linear model (1), it can be shown that the curvature dilatation is distributed as a mean Gaussian random field. Based on the kinematic equation (3), the rate of curvature change is given as a system of simultaneous partial differential equations (Drew, 1991, pp.

206-210) [14]:

$$\frac{\partial \kappa_i}{\partial t} = \kappa_i^2 V_{\mathbf{n}} + \Delta V_{\mathbf{n}},\ i = 1, 2,$$

where Δ is the Laplace-Beltrami operator on the cortical surface. For relatively small displacement velocity $\mathbf{V}$, the Laplacian can be neglected, i.e.

$$\frac{\partial \kappa_i}{\partial t} \approx \kappa_i^2 V_{\mathbf{n}},\ i = 1, 2. \tag{12}$$

Then it follows that $\Lambda_{curvature} \approx (\kappa_1^3 + \kappa_2^3) V_{\mathbf{n}}/K$. Under the assumption of (1), the normal velocity component becomes

$$V_{\mathbf{n}} = \mu_{\mathbf{n}} + \epsilon_{V_{\mathbf{n}}}, \tag{13}$$

where $\mu_{\mathbf{n}} = \langle \mu, \mathbf{n} \rangle$ is the mean normal velocity and $\epsilon_{V_{\mathbf{n}}}$ is a mean zero Gaussian random field. It follows that the curvature dilatation rate can be modeled as

$$\Lambda_{curvature}(\mathbf{x}) = \lambda_{curvature}(\mathbf{x}) + \epsilon_{curvature}(\mathbf{x}),$$

where $\lambda_{curvature}$ is the mean curvature dilatation rate and $\epsilon_{curvature}$ is a mean zero Gaussian random field. Afterwards, detecting the region of statistically significant curvature change can be performed via thresholding the maximum of the T random field defined on the cortical surface (Worsley *et al.*, 1996a; Worsley *et al.*, 1999).

The total bending energy of surface is computed as the integral over the surface $\partial\Omega_t$ of the local bending energy:

$$\int_{\partial\Omega_t} K(\mathbf{x})\, d\mathbf{x}.$$

A similar approach has been taken to measure the amount of bending in the 2D contour of the corpus callosum (Peterson *et al.*, 2001).

5 Surface-Based Diffusion Smoothing

In order to increase the signal-to-noise ratio (SNR) as defined in Dougherty (1999), Rosenfeld and Kak (1982) and Worsley *et al.* (1996c), Gaussian kernel smoothing is desirable in many statistical analyses . For example, Figure 3 shows fairly large variations in cortical thickness of a single subject displayed on the average brain atlas Ω_{atlas}. By smoothing the data

on the cortical surface, the SNR will increase if the signal itself is smooth and in turn, it will be easier to localize the morphological changes. However, due to the convoluted nature of the cortex whose geometry is non-Euclidean, we can not directly apply Gaussian kernel smoothing on the cortical surface. Gaussian kernel smoothing of functional data $f(\mathbf{x}), \mathbf{x} = (x_1, \ldots, x_n) \in \mathbb{R}^n$ with FWHM (*full width at half maximum*) $= 4(\ln 2)^{1/2}\sqrt{t}$ is defined as the convolution of the Gaussian kernel with f:

$$F(\mathbf{x}, t) = \frac{1}{(4\pi t)^{n/2}} \int_{\mathbb{R}^n} e^{-(x-y)^2/4t} f(y) dy. \tag{14}$$

Formulation (14) can not be directly to the cortical surfaces. However, by reformulating Gaussian kernel smoothing as a solution of a diffusion equation on a Riemannian manifold, the Gaussian kernel smoothing approach can be generalized to an arbitrary curved surface. This generalization is called *diffusion smoothing* and has been used in the analysis of fMRI data on the cortical surface (Andrade *et al.*, 2001). It can be shown that (14) is the integral solution of the n-dimensional diffusion equation

$$\frac{\partial F}{\partial t} = \Delta F \tag{15}$$

with the initial condition $F(\mathbf{x}, 0) = f(\mathbf{x})$, where $\Delta = \partial^2/\partial x_1^2 + \cdots + \partial^2/\partial x_n^2$ is the Laplacian in n-dimensional Euclidean space (Egorov and Shubin, 1991). Hence the Gaussian kernel smoothing is equivalent to the diffusion of the initial data $f(\mathbf{x})$ after time t. When applying diffusion smoothing on curved surfaces, the smoothing somehow has to incorporate the geometrical features of the curved surface and the Laplacian Δ should change accordingly. The extension of the Euclidean Laplacian to an arbitrary Riemannian manifold is called the *Laplace-Beltrami operator* (Arfken, 2000; Kreyszig, 1959). The approach taken in Andrade *et al.* (2001) is based on a local flattening of the cortical surface and estimating the planar Laplacian, which may not be as accurate as our estimation based on the finite element method (FEM). Further, our direct FEM approach completely avoid any local or global surface flattening. For given Riemannian metric tensor g_{ij}, the Laplace-Beltrami operator Δ is defined as

$$\Delta F = \sum_{i,j} \frac{1}{|g|^{1/2}} \frac{\partial}{\partial u^i} \Big(|g|^{1/2} g^{ij} \frac{\partial F}{\partial u^j} \Big), \tag{16}$$

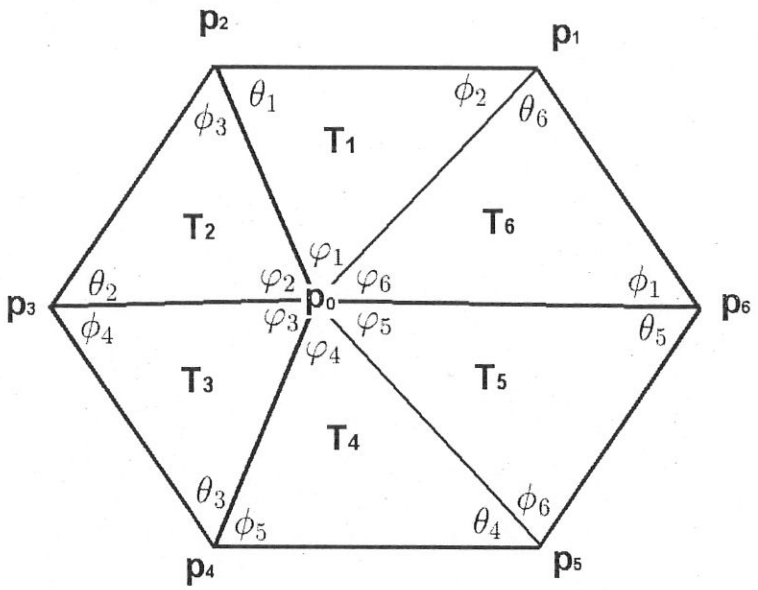

Figure 6: A typical triangulation in the neighborhood of $\mathbf{p} = \mathbf{p}_0$. When ASP algorithm is used, the triangular mesh is constructed in such a way that it is always pentagonal or hexagonal.

where $(g^{ij}) = g^{-1}$ (Arfken, 2000, pp. 158-167). Note that when g becomes a 2 $\times$2 identity matrix, the Laplace-Beltrami operator in (16), simplifies to a standard 2D Laplacian:

$$\Delta F = \frac{\partial^2 F}{\partial (u^1)^2} + \frac{\partial^2 F}{\partial (u^2)^2}.$$

Using the FEM on the triangular cortical mesh generated by the ASP algorithm, it is possible to estimate the Laplace-Beltrami operator as the linear weights of neighboring vertices (Chung, 2001).

Let $\mathbf{p}_1, \cdots, \mathbf{p}_m$ be m neighboring vertices around the central vertex $\mathbf{p} = \mathbf{p}_0$. Then the estimated Laplace-Beltrami operator is given by

$$\widehat{\Delta F}(p) = \sum_{i=1}^{m} w_i \big(F(\mathbf{p}_i) - F(\mathbf{p})\big)$$

with the weights

$$w_i = \frac{\cot \theta_i + \cot \phi_i}{\sum_{i=1}^{m} \|T_i\|},$$

where θ_i and ϕ_i are the two angles opposite to the edge connecting $\mathbf{p}_i$ and $\mathbf{p}$, and $\|T_i\|$ is the area of the i-th triangle (Figure 6). This is an improved formulation from the previous

attempt in diffusion smoothing on the cortical surface (Andrade *et al.*, 2001), where the Laplacian is simply estimated as the planar Laplacian after locally fattening the triangular mesh consisting of nodes $\mathbf{p}_0, \cdots, \mathbf{p}_m$ onto a flat plane. In the numerical implementation, we have used formulas

$$\cot\theta_i = \frac{\langle \mathbf{p}_{i+1} - \mathbf{p}, \mathbf{p}_{i+1} - \mathbf{p}_i \rangle}{2\|T_i\|}, \cot\phi_i = \frac{\langle \mathbf{p}_{i-1} - \mathbf{p}, \mathbf{p}_{i-1} - \mathbf{p}_i \rangle}{2\|T_i\|}$$

and $\|T_i\| = \|(\mathbf{p}_{i+1} - \mathbf{p}) \times (\mathbf{p}_i - \mathbf{p})\|/2$. Afterwards, the finite difference scheme is used to iteratively solve the diffusion equation at each vertex $\mathbf{p}$:

$$\frac{F(\mathbf{p}, t_{n+1}) - F(\mathbf{p}, t_n)}{t_{n+1} - t_n} = \widehat{\Delta} F(\mathbf{p}, t_n),$$

with the initial condition $F(\mathbf{p}, 0) = f(\mathbf{p})$. After N-iterations, the finite difference scheme gives the diffusion of the initial data f after duration $N\delta t$. If the diffusion were applied to Euclidean space, it would be equivalent to Gaussian kernel smoothing with

$$\text{FWHM} = 4(\ln 2)^{1/2}\sqrt{N\delta t}.$$

It should be emphasized that Gaussian kernel smoothing is a special case of diffusion smoothing restricted to Euclidean space. Computing the linear weights for the Laplace-Beltrami operator takes a fair amount of time (about 4 minutes in Matlab running on a Pentium III machine), but once the weights are computed, it is applied through the whole iteration repeatedly and the actual finite difference scheme takes only two minutes for 100 iterations.

6 Statistical Inference on the Cortical Surface

All of our morphological measures such as surface area, cortical thickness, curvature dilatation rates are modeled as Gaussian random fields on the cortical surface, i.e.

$$\Lambda(\mathbf{x}) = \lambda(\mathbf{x}) + \epsilon(\mathbf{x}), \mathbf{x} \in \partial\Omega_{atlas}, \tag{17}$$

where the deterministic part λ is the mean of the metric Λ and ϵ is a mean zero Gaussian random field. As we have explained earlier, we need to assume that $\mathbf{Var}(\epsilon)$ does not depends on time t. The T random field on the manifold $\partial\Omega_{atlas}$ is defined as

$$T(\mathbf{x}) = \sqrt{n}\frac{M(\mathbf{x})}{S(\mathbf{x})}, \ \mathbf{x} \in \partial\Omega_{atlas}$$

where M and S are the sample mean and standard deviation of metric Λ over the n subjects. Under the null hypothesis

$$H_0 : \lambda(\mathbf{x}) = 0 \text{ for all } \mathbf{x} \in \partial\Omega_{atlas},$$

i.e. no structural change, $T(\mathbf{x})$ is distributed as a student's t with $n-1$ degrees of freedom at each voxel x. The P value of the local maxima of the T field will give a conservative threshold, which has been used in brain imaging for a quite some time (Worsley, 1996a). For very high threshold y, we can show that

$$P\Big(\max_{\mathbf{x}\in\partial\Omega_{atlas}} T(\mathbf{x}) \geq y\Big) \approx \sum_{i=0}^{3} \phi_i(\partial\Omega_{atlas})\rho_i(y), \tag{18}$$

where ρ_i is the i-dimensional EC-density and the Minkowski functional ϕ_i are

$$\phi_0(\partial\Omega_{atlas}) = 2,\ \phi_1(\partial\Omega_{atlas}) = 0,\ \phi_2(\partial\Omega_{atlas}) = \|\partial\Omega_{atlas}\|,\ \phi_3(\partial\Omega_{atlas}) = 0$$

and $\|\partial\Omega_{atlas}\|$ is the total surface area of $\partial\Omega_{atlas}$ (Worsley, 1996a). When diffusion smoothing with given FWHM is applied to metric Λ on the atlas cortical s urface $\partial\Omega_{atlas}$, the 0-dimensional and 2-dimensional EC-density becomes

$$\rho_0(y) = \int_y^\infty \frac{\Gamma(\frac{n}{2})}{((n-1)\pi)^{1/2}\Gamma(\frac{n-1}{2})}\Big(1+\frac{y^2}{n-1}\Big)^{-n/2}\,dy,$$

$$\rho_2(y) = \frac{1}{\mathrm{FWHM}^2}\frac{4\ln 2}{(2\pi)^{3/2}}\frac{\Gamma(\frac{n}{2})}{(\frac{n-1}{2})^{1/2}\Gamma(\frac{n-1}{2})}y\Big(1+\frac{y^2}{n-1}\Big)^{-(n-2)/2}.$$

Therefore, the excursion probability on the cortical surface can be approximated by the following formula:

$$P\Big(\max_{\mathbf{x}\in\partial\Omega_{atlas}} T(\mathbf{x}) \geq y\Big) \approx 2\rho_0(y) + \|\partial\Omega_{atlas}\|\rho_2(y).$$

We compute the total surface area $\|\partial\Omega_{atlas}\|$ by summing the area of each triangle in a triangulated surface. The total surface area of the average atlas brain is 275,800 mm^2, which is roughly the area of 53×53 cm^2 sheet. We want to point out that the surface area of the average atlas brain is not the average surface area of 28 subjects. When 20mm FWHM diffusion smoothing is used on the template surface $\partial\Omega_{atlas}$, 2.5% thresholding gives

$$P\Big(\max_{\mathbf{x}\in\partial\Omega_{atlas}} T(\mathbf{x}) \geq 5.1\Big) \approx 0.025,$$

$$P\Big(\max_{\mathbf{x}\in\partial\Omega_{atlas}} T(\mathbf{x}) \leq -5.1\Big) \approx 0.025.$$

7 Results

Twenty-eight normal subjects were selected based on the same physical, neurological and psychological criteria described in Giedd *et al.* (1996a). This is the same data set reported in Chung *et al.* (2001), where the Jacobian of the 3D deformation was used to detect statistically significant brain tissue growth or loss in 3D whole brain via *deformation-based morphometry*. 3D Gaussian kernel smoothing used in this study is not sensitive to the interfaces between the gray, white matter and CSF. Gaussian kernel smoothing tends to blur gray matter volume increase data across the cortical boundaries. So in some cases, statistically significant brain tissue growth could be found in CSF. Tensor-based surface morphometry can overcome this inherent shortcoming associated with the previous morphometric analysis.

Two T_1-weighted MR scans were acquired for each subject at different times on the same GE Sigma 1.5-T superconducting magnet system. The first scan was obtained at the age 11.5 ± 3.1 years (min 7.0 years, max 17.8 years) and the second scan was obtained at the age 16.1 ± 3.2 years (min 10.6 years, max 21.8 years). The time difference between the first and the second scan was 4.6 ± 0.9 years (min time difference 2.2 years , max time difference 6.4 years). Using the automatic image processing pipeline (Zijdenbos *et al.*, 1998), MR images were spatially normalized into standardized stereotactic space via a global affine transformation (Talairach and Tournoux, 1988). Subsequently, an automatic tissue-segmentation algorithm based on an artificial neural network classifier was used to classify each voxel was as CSF, gray matter and white matter (Ozkan *et al.*, 1993). Afterwards, a triangular mesh for each cortical surface was generated by deforming a mesh to fit the proper boundary in a segmented volume using the ASP algorithm. For the first scan at time t_1, the outer cortical surface was triangulated in two steps: first, an ellipsoidal mesh placed outside the brain was shrunk down to the inner cortical surface, which is the white-gray matter boundary. The resulting mesh was used as the initial estimate in the second step that expands the mesh to fit the outer cortical surface, which is the gray-CSF boundary. To generate the outer surface for the second scan at time t_2, we start with the inner surface from the first scan taken at time t_1, and then expand it outward to match the outer surface on the classified volume of the second scan. Starting with the same mesh for the inner surface

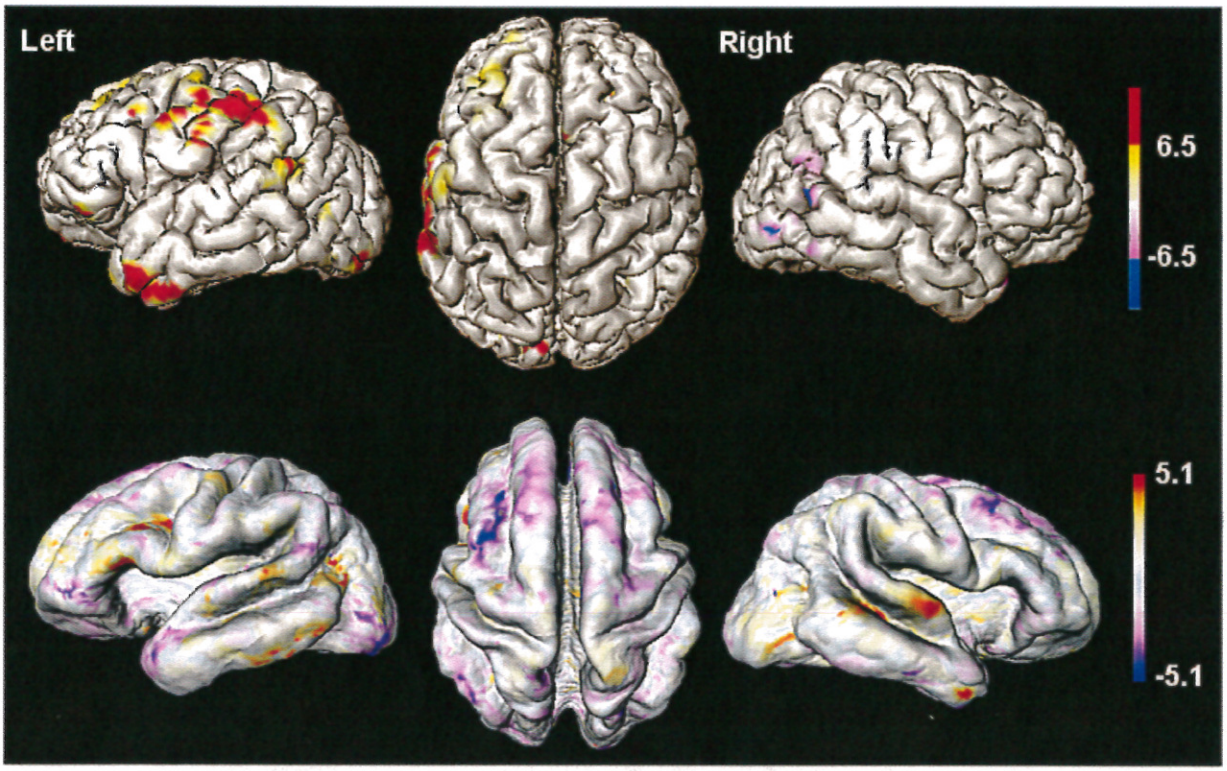

Figure 7: Top: t map of local gray matter change computed in 3D and then superimposed with an atlas brain. The predominant local gray matter volume increases were detected in somatosensory and motor cortex and temporal lobe. The left and right hemispheres show asymmetric growth pattern. Bottom: t map of the cortical surface area dilatation rate showing the statistically significant region of area expansion and reduction. The red regions are statistically significant surface area expansions while the blue regions are statistically significant surface area reductions between ages 12 and 16.

in the two expansion steps, each node in the initial mesh gets mapped to a point on the outer surface for each scan. This surface deformation method assumes that the shape of the cortical surface does not appreciably change within subject. This assumption is valid in the case of brain development for a short period of time as illustrated in Figure 1, where the global sulcal geometry remains stable for five year interval, although local cortical geometry shows some changes. This deformation technique may fail if we try to deform the inner surface of one subject to the outer surface of another subject. From this surface deformation technique, the displacement vector fields from the point on the outer surface of the first scan to the corresponding point on the second scan are obtained.

Gray matter volume change

The total gray matter volume dilatation rate $\Lambda^j_{total\ volume}$ for subject j was computed using

the triangular meshes that represents the outer and inner cortical surfaces. The mean total gray matter volume dilatation rate $\bar{\Lambda}_{total\ volume}$ was

$$\bar{\Lambda}_{total\ volume} = \frac{1}{n}\sum_{j=1}^{n} \Lambda^{j}_{total\ volume} = -0.0050.$$

This 0.5% annual decrease in the total gray matter volume is statistically significant (t value of -4.45). There has been substantial developmental studies on gray matter volume reduction for children and adolescents (Courchesne *et al*, 2000; Giedd *et al.*, 1999; Jernigan *et al.*, 1991; Pfefferbaum *et al.*, 1994; Rajapakse *et al.*, 1996; Riess *et al.*, 1996; Steen *et al.*, 1997). Our result confirms these studies. However, the ROI-based volumetry used in the previous studies did not allow investigators to detect local volume change within the ROIs. Our local volumetry based on deformation field can overcome the limitation of the ROI-based volumetry.

Brain tissue growth and loss based on the local volume dilatation rate was detected in the whole brain volume that includes both gray and white matter (Chung *et al.*, 2001). The morphometric analysis performed in Chung *et al.* (2001) generates 3D statistical parametric map (SPM) of brain tissue growth. By superposing the 3D SPM with the triangular mesh of the cortical surface of the atlas brain, we get gray matter volume change SPM restricted onto the cortical surface (Figure 7). Although it is an ad hoc approach, the resulting SPM projected on to the atlas brain seem to confirm some of the results in Giedd *et al.* (1999) and Thompson *et al.* (2000). In particular, Giedd *et al.* (1999) reported that frontal and parietal gray matters decrease but temporal and occipital gray matters increase even after age 12. In our analysis, we found local gray matter volume growth in the parts of temporal, occipital, somatosensory and motor regions but did not detect any volume loss in the frontal lobe. Instead we found statistically significant structural movements without accompanying volume decreases (Chung *et al.* 2001).

Surface area change

We measured the total surface area dilatation rate $\Lambda^{j}_{total\ area}$ for subject j by computing the total area of triangular meshes on the both outer and inner cortical surfaces. Then the mean

total area dilatation rate $\bar{\Lambda}_{totalarea}$ for $n = 28$ subjects was found to be

$$\bar{\Lambda}_{total\ area} = \frac{1}{n}\sum_{j=1}^{n} \Lambda^{j}_{total\ area} = -0.0094.$$

This 0.9% decrease of the total cortical surface area per year is statistically significant (t value of -9.25). Between the first scan taken at age 11.5 and the second scan taken at age 16.1, there was 4.3% decrease in the total cortical surface area.

In order to detect the regions of local surface area growth or reduction, the surface area dilatation rates were computed for all subjects, then smoothed with 20mm FWHM diffusion smoothing to increase the signal-to-noise ratio. Averaging over 28 subjects, local surface area change was found to be between -15.79% and 13.78% per year. In one particular subject, we observed between -106.5% and 120.3% of the local surface area change over 4 year time span. Figure 7 is the t map of the cortical surface area dilatation showing cortical tissue growth pattern. Surface area growth and decrease were detected by $T > 5.1$ and $T < -5.1$ ($P < 0.05$, corrected) respectively, showing statistically significant local surface expansion in Broca's area in the left hemisphere and local surface shrinkage in the left superior frontal sulcus. Most of surface reduction seems to be concentrated near the frontal region.

Cortical thickness change

The growth pattern of cortical thickness change is found to be very different but closely related to that of local surface area change. In the numerical implementation, the cortical thickness dilatation rate $\Lambda^{j}_{thickness}$ for subject j is given by the discrete approximation:

$$\Lambda^{j}_{thickness} = \frac{\|x(t_j) - y(t_j)\| - \|x(0) - y(0)\|}{t_j \|x(0) - y(0)\|},$$

where t_j is the time difference between two scans. Afterwards, the within average cortical thickness dilatation rate is computed by computing

$$\bar{\Lambda}^{j}_{thickness} = \frac{1}{\|\partial\Omega_{atlas}\|}\int_{x\in\partial\Omega_{atlas}} \Lambda^{j}_{thickness}(\mathbf{x})\ d\mathbf{x}.$$

The average cortical thickness dilatation rate across all within and between subjects was found to be

$$\bar{\Lambda}_{thickness} = \frac{1}{n}\sum_{j=1}^{n} \bar{\Lambda}^{j}_{thickness} = 0.025$$

This 2.5% annual increase (11.3% over 4.6 year time span) in the cortical thickness is statistically significant (t value of 17.7). Although there are regions of cortical thinning present in all individual subjects, our statistical analysis indicates that the overall global pattern of thickness increase is more predominant feature between ages 12 and 16. Also we localized the region of statistically significant cortical thickness increase by thresholding the t map of the cortical thickness dilatation rate by 5.1 (Figure 3). Cortical thickening is widespread on the cortex. The most predominant thickness increase was detected in the left superior frontal sulcus, which is the same location we detected local surface area reduction while local gray matter volume remains the same. So it seems that while there is no gray matter volume change, the left superior frontal sulcus undergoes cortical thickening and surface area shrinking and perhaps this is why we did not detect any local volume change in this region.

The most interesting result found so far is that there is almost *no* statistically significant local cortical thinning detected on the whole cortical surface between ages 12 and 16. As we have shown, the total inner and outer surface areas as well as the total volume of gray matter decrease. So it seems that all these results are in contradiction. However, if the rate of the total surface area decrease is faster than the rate of the total volume reduction, then it is possible to have cortical thickening. To see this, suppose we have a shallow solid shell with constant thickness h, total volume V and total surface area A. Then $V = hA$. It can be shown that the rate of volume change per unit volume can be written as $\dot{V}/V = \dot{h}/h + \dot{A}/A$. Using our dilatation notation, $\bar{\Lambda}_{total\ volume} = \bar{\Lambda}_{thickness} + \bar{\Lambda}_{total\ area}$. In our data, $\bar{\Lambda}_{total\ volume} = -0.0050 > \bar{\Lambda}_{total\ area} = -0.0094$, so we should have increase in the cortical thickness. However, we want to point out that this argument is only heuristic because the cortical thickness is not uniform across the cortex. Sowell *et al.* (2001) reported cortical thinning or gray matter density decrease in the frontal and parietal lobes in similar age group. The thickness measure they used is based on gray matter density, which measures the proportion of gray matter within a sphere with fixed radius between 5 to 15mm around a point on the outer cortical surface (Sowell *et al.*, 2001b; Thompson *et al.*, 2001). However, the gray matter density not only measures the cortical thickness but also the amount of bending. If a point is chosen on a gyrus, the increase in the bending energy will correspond to the increase in gray matter density. So the region of gray matter density decrease reported in

Sowell *et al.* (2001b) more closely resembles the region of curvature increase (Figure 5) than the region of cortical thickness change (Figure). Because they measure different anatomical quantities, it is hard to directly compare the result reported in Sowell *et al.* (2001b) to our result.

Curvature change: Our study is the first to use the curvature as the direct measure of anatomical changes in normal brain development. If a flat surface with bending energy $K = 0$ bends to a curved surface with $K > 0$ at a certain vertex, the curvature dilatation rate becomes infinite. To avoid such divergence in numerical computation, we have thresholded the bending energy to be $0.001 < K < 1$ and this range of curvature is sufficient to capture the bending of the cortex (Figure 5). Then we measured curvature dilatation rate $\Lambda^j_{curvature}$ for each subject j based on the thin plate bending energy. The within average curvature dilatation rate for each subject is defined as

$$\bar{\Lambda}^j_{curvature} = \frac{1}{\|\partial\Omega_{atlas}\|} \int_{\partial\Omega_{atlas}} \Lambda^j_{curvature}(\mathbf{x})\, d\mathbf{x}.$$

The average curvature dilatation rate across all within and between subjects was found to be

$$\bar{\Lambda}_{curvature} = \frac{1}{n} \sum_{j=1}^{n} \bar{\Lambda}^j_{curvature} = 2.50.$$

250% increase in total bending energy is statistically significant (t value of 19.42). Local curvature change was detected by thresholding the t statistic of the curvature dilatation rate at 5.1 (corrected). The superior frontal and middle frontal gyri show curvature increase. It is interesting to note that between these two gyri we have detected cortical thickness increase and local surface area decrease. It might be possible that cortical thickness increase and local surface area shrinking in the superior frontal sulcus causes the bending in the neighboring middle and superior frontal gyri. Such interacting dynamic pattern has been also detected in Chung *et al.* (2001), where gray matter tissue growth causes the inner surface to translate toward the region of white matter tissue reduction.

We also found *no* statistically significant local curvature decrease over whole cortex. While the gray matter is shrinking in both total surface area and volume, the cortex itself seems to get folded to give increasing curvature.

Conclusions

The surface-based morphometry presented here can quantify the rate of cortical thickness, area, curvature and the gray matter volume change at a local level without specifying the regions of interest (ROI). This ROI-free approach might be best suitable for exploratory whole brain morphometric studies. Because the approach is based on tensor geometry and parameterized surface, it successfully avoids artificial surface flattening (Andrade *et al.*, 2001; Angenent *et al.*, 1999), which can destroy the inherent geometrical structure of the cortical surface. It seems that any structural or functional analysis associated with the cortex can be performed without surface flattening if tensor geometry is used as a basic mathematical model. Riemannian metric tensor formulation gives us an added advantage that not only it can be used to measure intrinsic geometrical properties of the cortex but also it is used for generalizing Gaussian kernel smoothing on the cortex via diffusion smoothing. Since it is a direct generalization of Gaussian kernel smoothing, the diffusion smoothing should locally inherit many mathematical and statistical properties of Gaussian kernel smoothing applied to standard 3D whole brain volume. The diffusion smoothing algorithm written in Matlab is freely available for Montreal Neurological Institute (MNI) triangular mesh file format at http://www.stat.wisc.edu/ mchung/diffusion. The modification for any other triangular mesh can be easily done. We tried to combine and unify morphometric measurement, image smoothing and statistical inference in the same framework of tensor geometry. As an illustration of this powerful unified approach, we applied it to a group of normal children and adolescents to see if we can detect the region of anatomical changes in gray matter. It is found that the cortical surface area and gray matter volume shrinks, while the cortical thickness and curvature tends to increase between ages 12 and 16 with a highly localized area of cortical thickening and surface area shrinking found in the superior frontal sulcus at the same time. It seems that the increase in thickness and decrease in the superior frontal sulcus might cause increased folding in the middle and superior frontal gyri.

Our unified tensor-based surface morphometry can be also used as a tool for future investigations of neurodevelopmental disorders where surface analysis of either the cortex or brain substructures would be relevant.

Appendix

A. Rate of Metric Tensor Change

We will suppress spatial parameter $\mathbf{u}$ in $X(\mathbf{u}, t)$ and write it as $X(t)$ whenever there is no ambiguity. Then we have

$$X(t) = X(0) + \mathbf{U}(X(0), t). \tag{19}$$

Differentiating (19),

$$X_i(t) = X_i(0) + (\nabla \mathbf{U}) X_i(0),$$

where $\nabla \mathbf{U} = (\partial U_k / \partial x_l)$ is the 3×3 displacement gradient matrix defined in Chung *et al.* (2000). The metric tensor g_{ij} can be written as

$$\begin{aligned} g_{ij}(t) &= \langle X_i(t), X_j(t) \rangle & (20) \\ &= g_{ij}(0) + 2X_i^t(0)(\nabla \mathbf{U}) X_j(0) + X_i^t(0)(\nabla \mathbf{U})^t (\nabla \mathbf{U}) X_j(0), & (21) \end{aligned}$$

where ^{t} is the matrix transpose. For relatively small displacement, the higher order term involving $(\nabla \mathbf{U})^t (\nabla \mathbf{U})$ can be neglected:

$$g_{ij}(t) \approx g_{ij}(0) + 2X_i(0)^t (\nabla \mathbf{U}) X_j(0).$$

In the matrix form $g = (g_{ij})$, the rate of metric change is given by

$$\frac{\partial g}{\partial t} \approx 2(\nabla X)^t (\nabla \mathbf{V}) \nabla X,$$

where $\mathbf{V} = \partial \mathbf{U} / \partial t$ and $\nabla X = (X_1, X_2)|_{t=0}$ is a 3×2 gradient matrix evaluated at $t = 0$.

B. Rate of Cortical Thickness Change

Under deformation (19), the cortical thickness at $\mathbf{x}(t) \in \partial \Omega_t^{out}$ can be written as

$$\|\mathbf{x}(t) - \mathbf{y}(t)\| = \|\mathbf{x}(0) - \mathbf{y}(0) + \mathbf{U}(\mathbf{x}(0), t) - \mathbf{U}(\mathbf{y}(0), t)\|. \tag{22}$$

For relatively small displacement, we may neglect the higher order terms of $\mathbf{U}$ in the Taylor expansion of (22):

$$\|\mathbf{x}(t) - \mathbf{y}(t)\| \approx \|\mathbf{x}(0) - \mathbf{y}(0)\| + \left(\mathbf{U^t}(\mathbf{x(0)}, \mathbf{t}) - \mathbf{U^t}(\mathbf{y(0)}, \mathbf{t})\right) \frac{\mathbf{x(0)} - \mathbf{y(0)}}{\|\mathbf{x(0)} - \mathbf{y(0)}\|}. \tag{23}$$

Furthermore, $\mathbf{U}(\mathbf{x}(0),t) - \mathbf{U}(\mathbf{y}(0),t) \approx \nabla\mathbf{U}(\mathbf{x}(0),t)\big(\mathbf{x}(0)-\mathbf{y}(0)\big)$. Differentiating (23), we get

$$\frac{\partial}{\partial t}\|\mathbf{x}-\mathbf{y}\| \approx \big(\mathbf{x}(0)-\mathbf{y}(0)\big)(\nabla\mathbf{V})\frac{\mathbf{x}(0)-\mathbf{y}(0)}{\|\mathbf{x}(0)-\mathbf{y}(0)\|}.$$

If we let $\mathbf{d} = (d_1, d_2, d_3)^t = (\mathbf{x}(0)-\mathbf{y}(0))/\|\mathbf{x}(0)-\mathbf{y}(0)\|$, the thickness dilatation rate is given as a quadratic form in $\mathbf{d}$ such that

$$\frac{\partial}{\partial t}\ln\|\mathbf{x}-\mathbf{y}\| \approx \mathbf{d}^t(\nabla V)\mathbf{d} = \sum_{i,j=1}^{3} d_i d_j \frac{\partial^2 U_j}{\partial t \partial x_i}.$$

References

[1] R.J. Adler. *The Geometry of Random Fields.* John Wiley & Sons, 1981.

[2] A. Andrade, F. Kherif, J. Mangin, K.J. Worsley, A. Paradis, O. Simon, S. Dehaene, D. Le Bihan, and J-B Poline. Detection of fmri activation using cortical surface mapping. *Human Brain Mapping*, 12:79–93, 2001.

[3] S. Angenent, S. Hacker, A. Tannenbaum, and R. Kikinis. On the Laplace-Beltrami operator and brain surface flattening. *IEEE Transactions on Medical Imaging*, 18:700–711, 1999.

[4] G.B. Arfken. *Mathematical Methods for Physicists.* Academic Press, 5th. edition, 2000.

[5] A Bartesaghi and G. Sapiro. A system for the generation of curves on 3D brain images. *Human Brain Mapping*, 14:1–15, 2001.

[6] W.M. Boothby. *An Introduction to Differential Manifolds and Riemannian Geometry.* Academic Press, London, second edition edition, 1986.

[7] M.P. Do Carmo. *Riemannian geometry.* Prentice-Hall, Inc., 1992.

[8] M.K. Chung. *Statistical Morphometry in Computational Neuroanatomy.* Ph.D. thesis, McGill University, Montreal, Canada, 2001.

[9] M.K. Chung, K.J. Worsley, T. Paus, D.L. Cherif, C. Collins, J. Giedd, J.L. Rapoport, and A.C. Evans. A unified statistical approach to deformation-based morphometry. *NeuroImage*, 14:595–606, 2001.

[10] E. Courchesne, H.J. Chisum, J. Townsend, A. Cowles, J. Covington, B. Egaas, M. Harwood, S. Hinds, and G.A. Press. Normal brain development and aging : Quantitative analysis at in vivo MR imaging in healthy volunteers. *Radiology*, 216:672–682, 2000.

[11] A.M Dale and B. Fischl. Cortical surface-based analysis i. segmentation and surface reconstruction. *NeuroImage*, 9:179–194, 1999.

[12] C. Davatzikos and R.N. Bryan. Using a deformable surface model to obtain a shape representation of the cortex. In *Proceedings of the IEEE International Conference on Computer Vision*, pages 2122–2127, 1995.

[13] E.R. Dougherty. *Random Processes for Image and Signal Processing.* IEEE Press, 1999.

[14] D.A. Drew. *Theory of multicomponent fluids.* Springer-Verlag, New York, 1991.

[15] Y.V. Egorov and M.A. Shubin. *Partial Differential Equations I: Foundations of the Classical Theory.* Springer-Verlag, 1991.

[16] J.N. Giedd, J. Blumenthal, N.O. Jeffries, J.C. Rajapakse, A.C. Vaituzis, H. Liu, Y.C. Berry., M. Tobin, J. Nelson, and F.X. Castellanos. Development of the human corpus callosum during childhood and adolescence: a longitudinal MRI study. *Progress in Neuro-Psychopharmacology & Biological Psychiatry*, 23:571–588, 1999.

[17] J.N. Giedd, J.W. Snell, N. Lange, J.C. Rajapakse, D. Kaysen, A.C. Vaituzis, Y.C. Vauss, S.D. Hamburger, P.L. Kozuch, and J.L. Rapoport. Quantitative magnetic resonance imaging of human brain development: Ages 4-18. *Cerebral Cortex*, 6:551–160, 1996a.

[18] C.D. Good, I.S. Johnsrude, J. Ashburner, R.N. Henson, K.J. Friston, and R.S.J. Frackowiak. A voxel-based morphometric study of aging in 465 normal adult human brains. *NeuroImage*, 14:21–36, 2001.

[19] L.D. Griffin. The intrinsic geometry of the cerebral cortex. *Journal of Theoretical Biology*, 166:261–273, 1994.

[20] M.E. Gurtin and G.B. McFadden. *On the Evolution of Phase Boundaries.* Springer-Verlag, New York, 1991.

[21] D.A. Harville. *Matrix Algebra from a Statistician's Perspective.* Springer-Verlag, New York, 1997.

[22] C. Henery and T. Mayhew. The cerebrum and cerebellum of the fixed human brain: efficient and unbiased estimates of volumes and cortical surface areas. *J. Anat.*, 167:167–180, 1989.

[23] T.L. Jernigan, D.A. Trauner, J.R. Hesselink, and P.A. Tallal. Maturation of human cerebrum observed in vivo during adolescence. *Brain*, 114:2037–2049, 1991.

[24] S.E. Jones, B. R. Buchbinder, and I. Aharon. Three-dimensional mapping of cortical thickness using Laplace's equation. *Human Brain Mapping*, 11:12–32, 2000.

[25] S.C. Joshi, J. Wang, M.I. Miller, D.C. Van Essen, and U. Grenander. On the differential geometry of the cortical surface. *Vision Geometry IV, Vol. 2573, Proceedings of the SPIE's 1995 International Symposium on Optical Science, Engineering and Instrumentation*, pages 304–311, 1995.

[26] N. Kabani, G. Le Goualher, D. MacDonald, and A. C. Evans. Measurement of cortical thickness using an automated 3-d algorithm: A validation study. *NeuroImage*, 13:375–380, 2000.

[27] N. Khaneja, M.I. Miller, and U. Grenander. Dynamic programming generation of curves on brain surfaces. *IEEE Transactions on Pattern Analysis and Machine Intelligence*, 20(11):1260–1265, November 1998.

[28] E. Kreyszig. *Differential Geometry.* University of Toronto Press, Toronto, 1959.

[29] W.E. Lorensen and H.E. Cline. Marching cubes: A hight resolution 3D surface construction algorithm. *Computer Graphics*, 21:21, 1987.

[30] J.D. MacDonald, N. Kabani, D. Avis, and A.C. Evans. Automated 3-d extraction of inner and outer surfaces of cerebral cortex from MRI. *NeuroImage*, 12:340–356, 2000.

[31] M. Ozkan, B.M. Dawant, and R.J. Maciunas. Neural-network-based segmentation of multi-modal medical images: a comparative and prospective study. *IEEE Trans. Med. Imaging*, 12:534–544, 1993.

[32] T. Paus, A. Zijdenbos, K. Worsley, D.L. Collins, J. Blumenthal, J.N. Giedd, J.L. Rapoport, and A.C. Evans. Structural maturation of neural pathways in children and adolescents: In vivo study. *Science*, 283:1908–1911, 1999.

[33] B.S. Peterson, F.A. Feineigle, L.H. Staib, and J.C. Gore. Automated measurement of latent morphological features in the human corpus callosum. *Human Brain Mapping*, 12:232–245, 2001.

[34] A. Pfefferbaum, D.H. Mathalon, E.V. Sullivan, J.M. Rawles, and K.O. Zipursky, R.B.and Lim. A quantitative magnetic resonance imaging study of changes in brain morphology from infancy to late adulthood. *Archives of Neurology*, 51:874–887, 1994.

[35] J.C. Rajapakse, J.N. Giedd, C. DeCarli, J.W. Snell, A. McLaughlin, Y.C. Vauss, A.L. Krain, S. Hamburger, and J.L. Rapoport. A technique for single-channel MR brain tissue segmentation: Application to a pediatric sample. *Magnetic Resonance Imaging*, 14:1053–1065, 1996.

[36] A.L. Riess, M.T. Abrams, H.S. Singer, J.L. Ross, and M.B. Denckla. Brain development, gender and iq in children: A volumetric imaging study. *Brain*, 119:1763–1774, 1996.

[37] A. Rosenfeld and A.C. Kak. *Digital Picture Processing*, Vol. 2. Academic Press, Orlando, 1982.

[38] J.A. Sethian. *Level Set Methods and Fast Marching Methods.* Cambridge University Press, 1996.

[39] P. Shi. Point-tracked quantitative analysis of left ventricular surface motion from 3-D image sequences. *IEEE Transactions on Medical Imaging*, 19:36–50, 2000.

[40] E.R. Sowell, P.M. Thompson, K.D. Tessner, and A.W. Toga. Mapping continued brain growth and gray matter density reduction in dorsal frontal cortex: Inverse relationships

during postadolescent brain maturation. *The Journal of Neuroscience*, 21:8819–8829, 2001.

[41] R.G. Steeen, R.J. Ogg, W.E. Reddick, and P.B. Kingsley. Age-related changes in the pediatric brain:quantitative MR evidence of maturational changes during adolescence. *Am. J. Neuroradiol.*, 18:819–828, 1997.

[42] G. Subsol. Crest lines for curve-based warping. *Brain Warping*, pages 241–262, 1999.

[43] J. Talairach and P. Tournoux. Co-planar stereotactic atlas of the human brain: 3-dimensional proportional system. an approach to cerebral imaging. *Thieme, Stuttgart*, 1988.

[44] P.M. Thompson, J.N. Giedd, R.P. Woods, D. MacDonald, A.C. Evans, and A.W. Toga. Growth patterns in the developing human brain detected using continuum-mechanical tensor mapping. *Nature*, 404:190–193, 2000.

[45] P.M. Thompson, M.S. Mega, R.P. Woods, C.I. Zoumalan, C.J. Lindshield, R.E. Blanton, J. Moussai, C.J. Holmes, J.L. Cummings, and A.W. Toga. Cortical change in Alzheimer's disease detected with a disease-specific population-based brain atlas. *Cerebral Cortex*, 11:1–16, 2001.

[46] K. J. Worsley, M. Andermann, T. Koulis, D. MacDonald, and A. C. Evans. Detecting changes in non-isotropic images. *Human Brain Mapping*, 8:98–101, 1999.

[47] K.J. Worsley, S. Marrett, P. Neelin, and A.C. Evans. Searching scale space for activation in pet images. *Human Brain Mapping*, 4:74–90, 1996.

[48] K.J. Worsley, S. Marrett, P. Neelin, A.C. Vandal, K.J. Friston, and A.C. Evans. A unified statistical approach for determining significant signals in images of cerebral activation. *Human Brain Mapping*, 4:58–73, 1996.

[49] A.P. Zijdenbos, A. Jimenez, and A.C Evans. Pipelines: Large scale automatic analysis of 3D brain data sets. *NeuroImage*, 7S:783, 1998.